ACS OMEGA

Open Access

http://pubs.acs.org/journal/acsodf

Article

Cotton-Like Three-Dimensional $Sb_4O_5Cl_2$ Structures: Synthesis and Ammonium Hydroxide Sensing

Rosimara P. Toledo,* Rosana A. Gonçalves, Maurício R. Baldan, and Olivia M. Berengue

Cite This: *ACS Omega* 2023, 8, 41295−41301

Read Online

ACCESS | Metrics & More | Article Recommendations | Supporting Information

ABSTRACT: Nanostructured materials have emerged as valuable tools for the advancement of novel electrocatalysts. Among them, three-dimensional metal oxides have gained significant attention due to their excellent conductivity, cost-effectiveness, and unique design. This study focuses on the synthesis of cotton-like three-dimensional antimony oxychloride ($Sb_4O_5Cl_2$) structures through a straightforward precipitation method. The nanostructures exhibit immense potential for sensing applications. Electrochemical characterization reveals that the $Sb_4O_5Cl_2$ heterostructure demonstrates a remarkable double-layer capacitance of 662 F/cm^2, accompanied by excellent cyclic stability. The sensor's performance was tested for the detection of ammonium hydroxide (HA) in NaCl solution, yielding sensitivities ranging from 0.95 to 0.140 mA mM^{-1} cm^{-2} and a detection limit of 4.54 μM within a wide detection range of 0.3−250 mM. The sensor device possesses a distinctive cotton-like structure and is synthesized through a simple and cost-effective route.

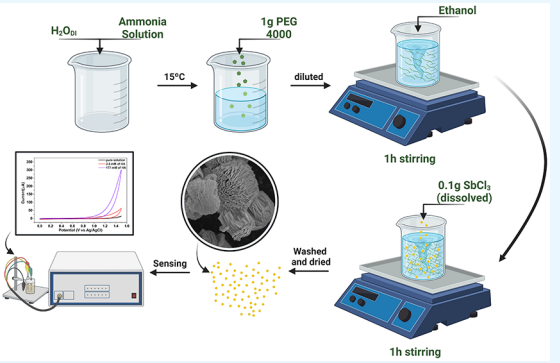

INTRODUCTION

The field of nanomaterials has recently witnessed significant attention, owing to the development of new technologies that offer faster, more sensitive, and highly efficient sensors, optoelectronics, and energy storage devices. The properties of nanostructures, including size, crystalline phase, and morphology, are influenced by various factors such as reagents employed, synthesis methodology, and reaction conditions.[1−4] By carefully adjusting the synthesis parameters such as temperature, pH, reagent concentration, synthesis time, and cleaning, it becomes feasible to tailor nanostructures with specific properties for targeted applications.[1,5−9]

Antimony oxychloride ($Sb_4O_5Cl_2$) is a material commonly synthesized in the monoclinic phase, offering intriguing optical, electrical, and mechanical properties.[10−12] It possesses a high melting point, excellent thermal stability, and good electrical conductivity, making it a compelling candidate for applications in flame-retardant materials, catalysts, degradation processes, sensors, and battery anodes.[11−14] Notably, Yang et al.[15] synthesized hollow microspheres of $Sb_4O_5Cl_2$ through a hydrothermal method, demonstrating its exceptional catalytic performance for Rhodamine B (RhB) and gaseous isopropanol (IPA). Additionally, Shi et al.[16] utilized the hydrothermal method to synthesize 3D flowerlike $Sb_4O_5Cl_2$ structures, which exhibited promising potential as anode materials in alkali metal-ion batteries. Despite the promising applications of antimony oxychloride, it has received limited attention, and the lack of novel morphologies has hindered its progress in technology-based applications.

Three-dimensional structures have proven successful in the development of electrochemical and gas sensors.[17−19] Various materials, including organic compounds such as PANI[20,21] and PPy,[22] as well as metal oxides like MoO_{3-x}/Egaln,[23] $GeSe_xO_y$,[24] CoVO/MXene,[25] $GaSe_{0.58}O_{0.42}$,[26] ZnO,[27,28] Mn_3O_4,[29,30] ZnO/NiO,[31] AlOOH,[32] and WO_3,[33] have been employed for this purpose. Due to their large surface area, these structures have enabled enhanced sensitivity and selectivity in detecting trace amounts of ammonium hydroxide (HA),[34,35] an aqueous solution of ammonia (NH_3) characterized by its colorless appearance and strong odor. HA is highly toxic and can cause skin burns and severe damage to the respiratory system. It finds applications in cleaning industries, fertilizer production, drug manufacturing, and as a cleaning agent for equipment and surfaces in the food industry.[36,37] In the meat industry, HA is used to raise pH levels and eliminate *Escherichia coli* bacteria.[38] Therefore, the detection of HA holds utmost importance, as it directly affects human lives, encompassing aspects such as quality control in industrial processes, analysis of water and air, and leak detection. The established maximum exposure limit is 25 ppm.[37,39]

Received: July 5, 2023
Accepted: September 7, 2023
Published: October 23, 2023

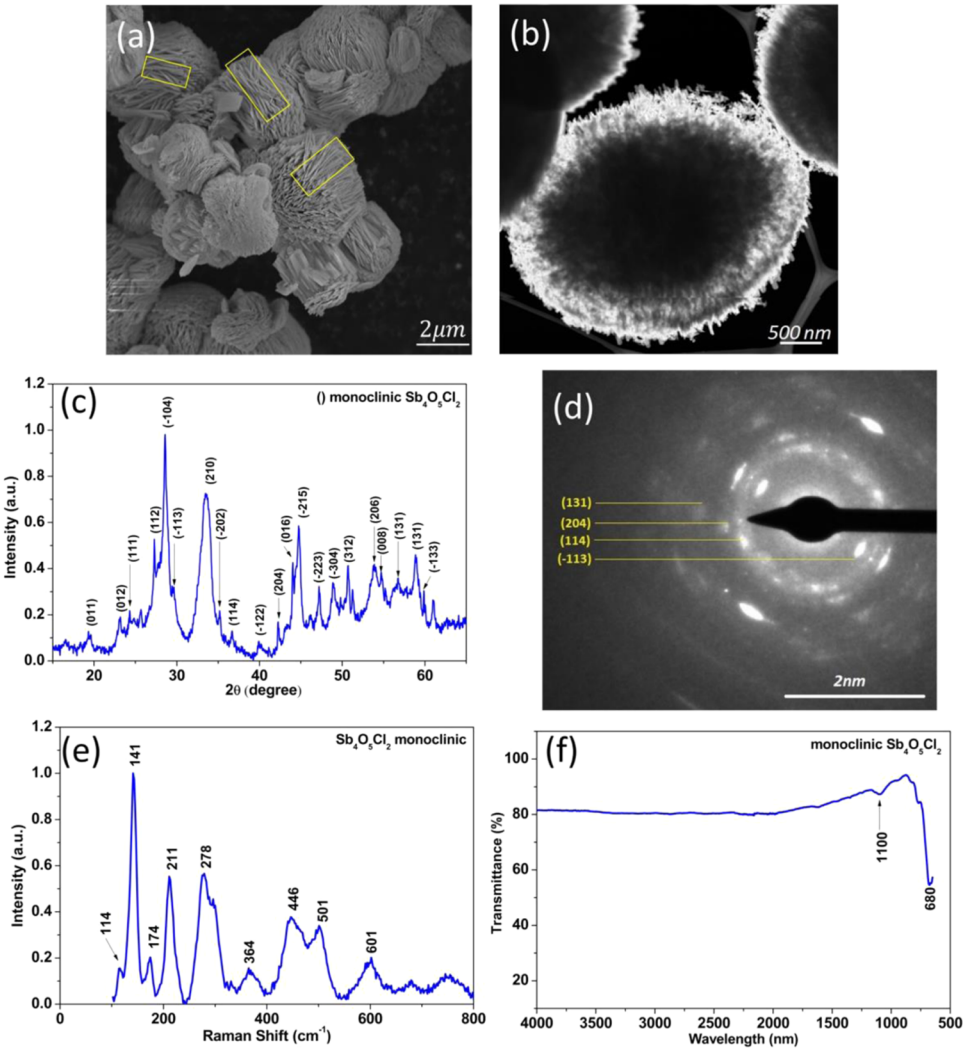

Figure 1. Structural characterization of the $Sb_4O_5Cl_2$ cotton-like three-dimensional structures: (a) SEM and (b) TEM of the $Sb_4O_5Cl_2$ samples, and (c) X-ray diffraction pattern, (d) SAED images with concentric rings showing different orientations, (e) Raman spectrum, and (f) FTIR spectra of the samples.

In this study, we present the synthesis of three-dimensional monoclinic antimony oxychloride structures using a facile precipitation method. Notably, the morphology achieved through this synthesis approach has not been reported in the literature for $Sb_4O_5Cl_2$. The microstructures were extensively characterized by using FE-SEM, TEM, SAED, XRD, Raman, and FTIR techniques to evaluate their morphology, phase composition, and crystal quality. Subsequently, these microstructures were employed for the detection of the contaminant ammonium hydroxide utilizing cyclic voltammetry and amperometric measurements. The results demonstrate high sensitivity toward minute concentrations of the contaminant and electrode stability upon reuse.

EXPERIMENTAL SECTION

Materials and Chemicals. The following reagents were used in the synthesis of the 3D $Sb_4O_5Cl_2$ structures. Ammonia solution (2.0 M in ethanol) and PEG-4000 were purchased from Sigma-Aldrich. Ethanol (C_2H_5OH, reagent grade, ≥99.8%), antimony chloride ($SbCl_3$, reagent grade, ≥99.8%), and ammonium hydroxide (24−26% PA) were purchased from Honeywell, Alfa Aesar, and Exodo, respectively. Ultrapure deionized water (≥18 MΩ cm) was obtained using a GEHAKA Master System All setup. Nitrogen purge gas (99.999% purity) for the electrochemical experiments was purchased from White Martins. All reagents were acquired from chemical industries and used without further purification.

Synthesis. The synthesis of the three-dimensional $Sb_4O_5Cl_2$ structures was carried out using a precipitation process.[40] Initially, 5 mL of deionized water (DI) and 2.5 mL of ammonia were mixed at room temperature, followed by cooling the mixture to 15 °C under vigorous mechanical stirring. Subsequently, 1 g of PEG-4000 was added, and after complete dissolution of PEG, 5 mL of ethanol was introduced to the synthesis vessel. The mixture was stirred for 1 h. Then, 100 mg of $SbCl_3$ dissolved in 2 mL of ethanol was added dropwise to the mixture and left stirring for an additional hour. The resulting mixture was allowed to stand for 3 h, filtered using a Whatman no. 4 filter paper (pore size 20−25 μm), and washed with ample amounts of water and ethanol. The obtained product was dried at 60 °C for 72 h.

Structural and Morphological Characterization. The morphology of the obtained nanostructures was investigated by field emission scanning electron microscopy (FE-SEM) with a secondary electron detector and transmission electron

https://doi.org/10.1021/acsomega.3c04751
ACS Omega 2023, 8, 41295−41301

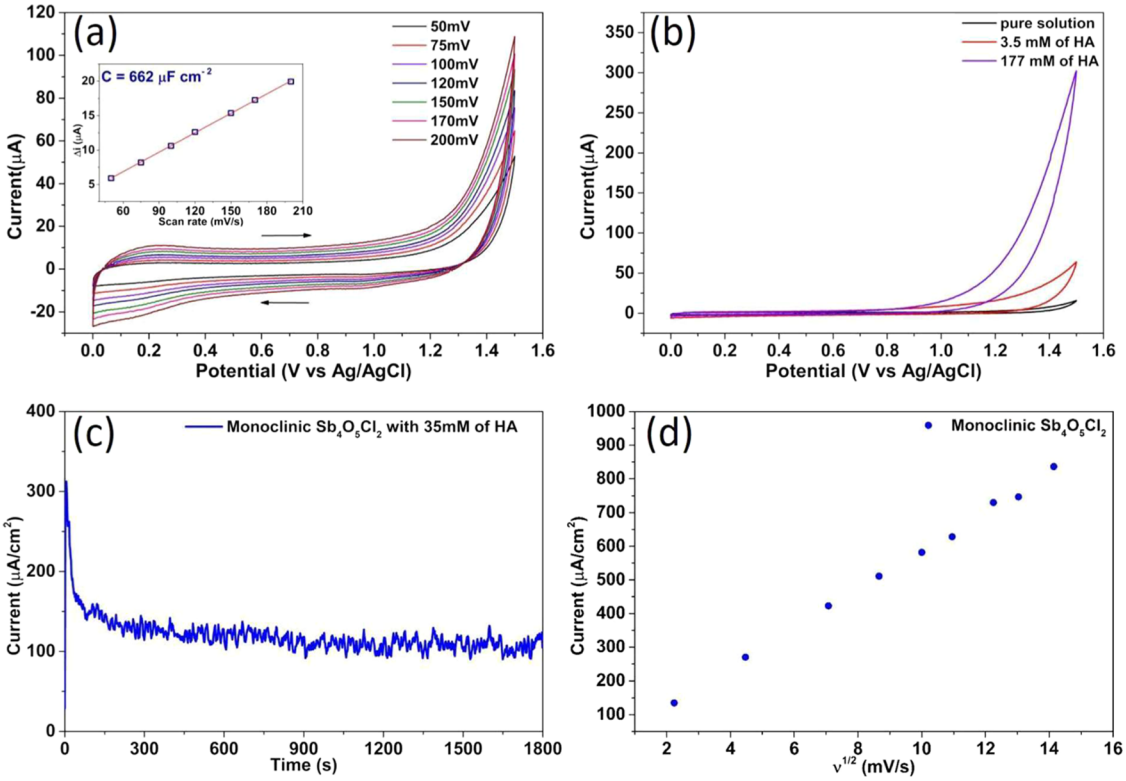

Figure 2. (a) Cyclic voltammograms of $Sb_4O_5Cl_2$ at different scan rates. The inset shows the plot of $2\Delta i$ versus the scan rate and the linear fitting used to determine the specific capacitance. (b) Comparative CV profiles of HA oxidation on the $Sb_4O_5Cl_2$ electrode. (c) Chronoamperometry measurement in a 0.1 M NaCl + 35 mM HA solution on the $Sb_4O_5Cl_2$ electrode. (d) Plot of current (I) versus scan rate square root obtained from VC experiments in a 0.1 M NaCl + 35 mM HA solution.

microscopy (TEM) for bright and dark field imaging. The FE-SEM analysis was performed using a TESCAN model MIRA 3 instrument, while the TEM analysis was carried out using a Tecnai model G2-F20 instrument.

The structural and crystalline phase analysis was conducted by X-ray diffractometry (XRD) using a PANalytical X'Pert Pro diffractometer equipped with a Cu Kα tube (λ = 1.540 Å) and a step scan of 0.02°. Selected area electron diffraction (SAED) was used to complement the XRD analysis.

Raman spectroscopy and attenuated total reflection infrared spectroscopy (ATR-FTIR) were employed for the optical characterization and compositional verification of the samples. Raman spectroscopy measurements were performed using the Horiba LabRAM HR Evolution spectrometer in a back-scattering geometry configuration equipped with a 514.5 nm line of an Ar+ laser at room temperature. The ATR-FTIR spectra were collected using a PerkinElmer Spectrum 100 instrument in the range of 600−4000 cm^{-1}.

Electrochemical Measurements. The electrochemical experiments were conducted in a conventional three-electrode electrochemical cell, utilizing a Ag/AgCl electrode (saturated NaCl) as the reference electrode, a gold (Au) spiral wire as the counter electrode, and a modified glassy carbon electrode as the working electrode.

The preparation of the working electrode involved polishing the glassy carbon surface with alumina paste (0.05 μm) and deionized water. A thin film of the material was then applied to the mirror surface of the glassy carbon electrode by pipetting suitable amounts of a suspension of the material in isopropyl alcohol (mass ratio 3:1) and allowing it to dry at room temperature. The estimated material loading on the electrode was 83.3 $\mu g/cm^2$.

All electrochemical measurements were performed using a diluted 0.1 mol/L NaCl aqueous solution as the supporting electrolyte at room temperature under a constant flow of N_2 gas to prevent the dissolution of atmospheric oxygen. Cyclic voltammetry (CV) and chronoamperometry experiments were carried out using a Princeton Applied Research potentiostat (PAR 283) controlled by Power Suite software. Current densities were calculated with respect to the geometric area of the working electrode (0.071 cm^2).

RESULTS AND DISCUSSION

Morphological and Structural Characterization. As a first step in characterizing the as-grown material, the morphology of the structures was examined by using FE-SEM and TEM techniques.

Figure 1a shows that the synthesized products are rounded cotton-like three-dimensional structures composed of aggregated petals (highlighted in Figure 1a) that resemble a rosebud in the micrograph. The TEM image in Figure 1b reveals that the cotton-like structures have micrometric dimensions (diameter ranging from 1.6 to 4.4 μm), while the composing petals are nanosized and thick (28−78 nm). The nanometric dimensions of the petals, combined with the presence of void spaces, contribute to the increased surface area of the cotton-like structures, which is desirable for various applications. Lakshmi et al.[41] and Jiang et al.[42] recently reported the synthesis of three-dimensional spherical structures of Sb_2S_3/$Sb_4O_5Cl_2$ and $Sb_4O_5Cl_2$, respectively, using the hydrothermal

https://doi.org/10.1021/acsomega.3c04751
ACS Omega 2023, 8, 41295−41301

method. This suggests that the unique morphology observed in our study results from precipitation in an acidic medium.

The XRD pattern of the as-grown material is shown in Figure 1c. The diffraction peaks correspond to the monoclinic $Sb_4O_5Cl_2$ phase (JCPDS 01-073-1534) with lattice parameters a = 6.229 Å, b = 5.107 Å, and c = 13.500 Å and the $P21/c$ (no. 14) space group.[15,43] The sharp and strong diffraction peaks indicate good crystalline quality, while the peak broadening, as shown in Figure 1c, can be attributed to the nanometric thickness of the petals in the cotton-like structures, known as "size broadening".[44] The SAED pattern in Figure 1d confirms the presence of concentric rings, indicating that the sample is composed of monocrystalline particles with different orientations, consistent with the XRD analysis. The crystalline planes detected in the SAED pattern also correspond to monoclinic $Sb_4O_5Cl_2$, confirming the sample composition. To the best of our knowledge, this is the first report on the synthesis of cotton-like three-dimensional structures of $Sb_4O_5Cl_2$ in the literature.

The Raman spectra of the as-synthesized samples are shown in Figure 1e. The spectrum exhibits sharp peaks at 114, 141, and 174 cm^{-1}, which are associated with the Sb−Cl stretching vibrations, while the peaks between 211 and 601 cm^{-1} are related to the Sb−O bond vibrations of the $Sb_4O_5Cl_2$ structures. These results are in agreement with the previous report by Shi et al.[13] and further confirm the XRD and SAED findings. Subsequently, FTIR characterization was performed to analyze the composition and detect possible residual organic molecules on the sample surface. The FTIR spectrum of the as-grown $Sb_4O_5Cl_2$ (Figure 1f) shows high transmittance (≥80%) across a wide spectral range (1000−4000 cm^{-1}). The peaks at 650 and 1100 cm^{-1} are associated with the stretching vibrations of Sb−O.[45] The absence of additional peaks in both the Raman and FTIR spectra indicates that the structures have clean surfaces without residual organic compounds or PEG radicals, confirming the efficiency of the synthesis and the quality of the obtained samples.

Electrochemical characterization. Based on the morphological and structural characteristics mentioned above, it is important to highlight that despite the toxicity of the material, these unique characteristics were exploited in the development of the device. In this context, tests were conducted to evaluate the performance of this device in detecting ammonium hydroxide (HA) using the cotton-like structures as the basis. Prior to evaluating the detection properties of $Sb_4O_5Cl_2$ for HA, cyclic voltammetry studies were performed on the cotton-like structures in a 0.1 M NaCl solution to obtain intrinsic information about the as-grown material (Figure 2a).

Figure 2b shows the CV curves obtained for $Sb_4O_5Cl_2$ in this supporting electrolyte at scanning rates ranging from 50 to 200 mV/s. The CV curves of the cotton-like structures exhibit similar behavior at all scan rates, without any peaks within the potential window, indicating a pseudocapacitive material.[46,47] From the Gileadi method,[48] these measurements estimate the double-layer capacitance of $Sb_4O_5Cl_2$ to be 662 $\mu F/cm^2$ (the inset in Figure 2a). This value indicates that $Sb_4O_5Cl_2$ has a good charge retention capacity compared to other oxides reported in the literature, such as β-MnO_2,[49] Co_3O_4,[50] $MoSe_2$,[51] TiO_2,[52] and CH_3CuS[53] (Table S1). To the best of our knowledge, this is the first report on the double-layer capacitance of $Sb_4O_5Cl_2$ in the literature.

Subsequently, the response of the $Sb_4O_5Cl_2$ electrode for the detection of ammonium hydroxide (HA) was investigated by using cyclic voltammetry and chronoamperometry studies. Figure 2b shows the CV curves obtained with different fractions of HA diluted in a 0.1 M NaCl solution for $Sb_4O_5Cl_2$. The measurements indicate an increase in the current density proportional to the addition of HA in the solution for potentials greater than 1.1 V. For example, when the HA fraction in the solution increases from 0 to 35 mM, the current density becomes approximately 300% higher compared to that in the pure solution. These data suggest the good capability of $Sb_4O_5Cl_2$ to detect HA.

Chronoamperometry experiments at a fixed potential (1.4 V) were also performed to evaluate the electrocatalytic activity of the $Sb_4O_5Cl_2$ electrode (Figure 2c). The long-term experiment demonstrates that the material maintains an almost constant charge density of 110 $\mu A/cm^2$ after 30 min of polarization, indicating good stability. Additionally, Figure 2d shows a linear correlation between the current density and the square root of the scan rate, indicating that the mass transport mechanism at the electrode interface is diffusion-controlled (Figure S2), following the Randles−Sevcik equation.[54−56]

Based on the excellent activity of the cotton-like three-dimensional structures for HA detection, the material was tested as an amperometric sensor. The calibration curve was constructed by measuring the current in chronoamperometry experiments at a fixed potential (1.4 V) after 180s of HA addition in the supporting electrolyte (Figure 3).

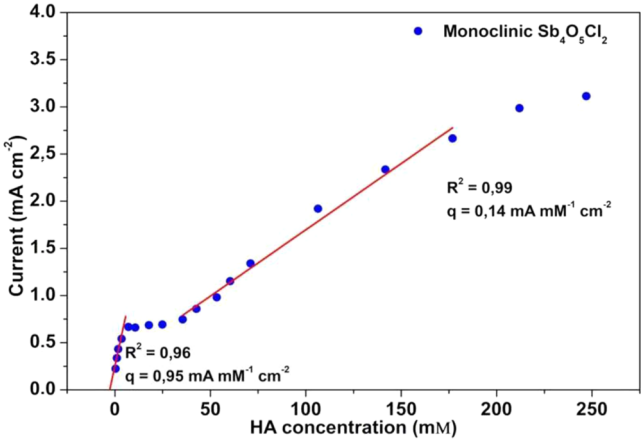

Figure 3. Calibration curve for HA detection on the Sb_4O_5Cl electrode.

Remarkably, the current exhibits a linear response to the HA concentration in two distinct regions: the first region at low HA concentrations, between 0.3 and 3.6 mM, shows higher sensitivity (q = 0.95 mA mM^{-1} cm^{-2}), while the second region at higher HA concentrations, between 43 and 177 mM, shows lower sensitivity (q = 0.14 mA mM^{-1} cm^{-2}). The correlation factor R^2 calculated for both regions is greater than 0.96, indicating a good fit of the model to the experimental data. The detection limit of HA was determined to be 4.5 μM/L using the method described by da Silva et al.[57]

Rahman et al. have investigated ammonia hydroxide sensors based on β-Fe_2O_3[58] and CuO.ZnO nanoparticles.[59] Both studies utilized a Pd wire as the counter electrode and Au and Ag electrodes coated with nanoparticles as the working electrodes in a phosphate buffer solution (PBS), respectively. The sensitivity of the nanoparticles for ammonia hydroxide obtained in the chemical sensor was 0.530 μA mM^{-1} cm^{-2} for

https://doi.org/10.1021/acsomega.3c04751
ACS Omega 2023, 8, 41295−41301

β-Fe_2O_3 and 1.549 μA mM^{-1} cm^{-2} for CuO.ZnO (both from the 0.77 μM to 0.77 M ammonia hydroxide fraction). The detection limits were 21.8 μM for β-Fe_2O_3 and 8.9 μM for CuO.ZnO. It is noteworthy that the cotton-like three-dimensional $Sb_4O_5Cl_2$ structures exhibit enhanced sensing activity compared to these materials. In both cases, Rahman et al. describe the detection of the contaminant based on oxidation or reduction processes of the sensor materials depending on the presence of dissolved oxygen in the medium. The described reduction process emphasizes that the studied materials capture electrons from the solution, causing the materials' resistance to decrease and, consequently, causing an increase in conductivity.[58,59]

We believe a similar process occurs for $Sb_4O_5Cl_2$, where the detection of HA can be described through oxidation and reduction reactions that occur on the surface of the film deposited on the GC electrode. The electrochemical reaction of NH_4OH molecules occurs at the working electrode, producing elements such as nitrogen, hydrogen ions, hydroxide, and electrons through the oxidation of HA.[60,61] Meanwhile, water molecules are formed at the counter electrode through the reaction with the released oxygen from the working electrode. The cotton-like three-dimensional $Sb_4O_5Cl_2$ structures exhibit high sensitivity and detection limit values compared to those reported for other oxide-based HA sensors, owing not only to their composition, which includes 5 oxygens, but also to their large surface area. Table 1 presents a comparison of the values obtained in this work to those found in the literature.

Table 1. Sensitivity and Detection Limit the Performance of the Reported HA Sensors

materials	sensitivity	detection limit	reference
$Sb_4O_5Cl_2$ microstructures	0.950 mA mM^{-1} cm^{-2}	4.54 μM	this work
	0.140 mA mM^{-1} cm^{-2}		
PtCu	9.400 μA μM^{-1} cm^{-2}	8.6 nM	62
β-Fe_2O_3 NPs	0.530 μA mM^{-1} cm^{-2}	21.8 μM	58
CuO codoped ZnO	1.549 μA mM^{-1} cm^{-2}	8.9 μM	59
α-Fe_2O_3 nanoellipsoids	4.678 μA mM^{-1} cm^{-2}	40 μM	63
Ag-CNT	0.613 mA mM^{-1} cm^{-2}	1 μM	64

Notably, the sensor reported here has the additional advantage of exhibiting a higher sensitivity at low HA concentrations and does not have an upper saturation limit, indicating that this sensor could be efficiently used across a wide range of concentrations. Stability and reproducibility are important parameters for practical applications, and tests were conducted to evaluate these electrode characteristics (Figure 4).

Cyclic voltammetry experiments were first performed in a 0.1 M NaCl + 35 mM HA solution using the same electrode. Between measurements, the electrode was removed from the cell and gently rinsed with deionized water to eliminate any reaction byproducts adsorbed on the surface. The reuse tests demonstrate good charge retention even after six consecutive measurements, indicating that the catalyst on the surface did not show any deactivation, thus maintaining its stability.[65,66] These results provide a new perspective and expand the field of developing novel sensors for the detection of ammonia hydroxide and indicate the excellent sensitivity of these samples in detecting HA, making this material promising for future applications in detection devices.

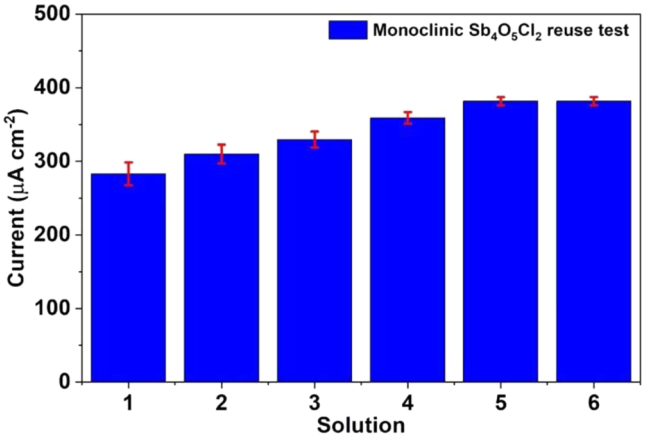

Figure 4. Reuse test conducted from CV experiments on the $Sb_4O_5Cl_2$ electrode in a 0.1 M NaCl + 35 mM HA solution.

CONCLUSIONS

The cotton-like three-dimensional $Sb_4O_5Cl_2$ structures were obtained through the precipitation method, which is a simple and cost-effective approach. The XRD and Raman analyses confirmed the presence of a monoclinic phase with good crystallinity, while the FE-SEM and SAED images revealed a nanometric size and a large surface area. The $I-V$ analysis demonstrated a significant change in surface current upon each injection of the target component into the bulk solution, indicating a detection limit (4.54 μM) and sensitivity (0.950 and 0.140 mA mM^{-1} cm^{-2}) that are in good agreement with the values reported for other oxide-based HA sensors. The $Sb_4O_5Cl_2$ electrode exhibited good charge retention. These findings suggest promising applications of this material in various fields and contribute to the advancement of its potential use.

ASSOCIATED CONTENT

Supporting Information

The Supporting Information is available free of charge at https://pubs.acs.org/doi/10.1021/acsomega.3c04751.

Table with a comparison of the charge retention capacity of different oxides found in the literature, zoom from 0.6 to 1.3 V of the comparative CV profiles of HA oxidation on the $Sb_4O_5Cl_2$ electrode (from Figure 2b), and the plot of log current (I) versus log scan rate square root obtained from VC experiments in a 0.1 M NaCl + 35 mM HA solution (PDF)

AUTHOR INFORMATION

Corresponding Author

Rosimara P. Toledo − *Department of Physics, School of Engineering and Sciences, São Paulo State University (UNESP), Guaratinguetá, São Paulo 12516-410, Brazil;* orcid.org/0000-0002-7029-2382; Email: rosimara.passos@gmail.com

Authors

Rosana A. Gonçalves − *Instituto Federal do Norte de Minas (IFNMG), Montes Claros, Minas Gerais 39480-000, Brazil*

https://doi.org/10.1021/acsomega.3c04751
ACS Omega 2023, 8, 41295−41301

Maurício R. Baldan − *PDM3A − Department of Space Engineering and Technology, National Institute of Space Research (INPE), São José dos Campos, São Paulo 12227-010, Brazil*

Olivia M. Berengue − *Department of Physics, School of Engineering and Sciences, São Paulo State University (UNESP), Guaratinguetá, São Paulo 12516-410, Brazil*

Complete contact information is available at: https://pubs.acs.org/10.1021/acsomega.3c04751

Notes

The authors declare no competing financial interest.

■ ACKNOWLEDGMENTS

R.P.T. is thankful to the Coordenação de Aperfeiçoamento de Pessoal de Nível Superior − Brasil (CAPES) − Finance Code 001, Professor Dr. Ronaldo S. Nunes, and Professor Dr. Roberto Z. Nakazato for support and access to electrochemical measurements; and to the Structural Characterization Laboratory (LCE) − UFSCar for access to the TEM facility.

■ REFERENCES

(1) Wang, X.; Jiang, Y.; Zhao, P.; Meng, X. Hierarchical structure and electronic effect promoted degradation of phenols over novel MnO2 nanoprisms via non-radical mechanism. *Sep. Purif. Technol.* **2022**, *303*, 122265.

(2) Geng, J.; Lu, D.; Zhu, J.-J.; Chen, H.-Y. Antimony (III)-doped PbWO4 crystals with enhanced photoluminescence via a shape-controlled sonochemical route. *J. Phys. Chem. B* **2006**, *110*, 13777−13785.

(3) Rao, C. N. R.; Vivekchand, S.; Biswas, K.; Govindaraj, A. Synthesis of inorganic nanomaterials. *Dalton Trans.* **2007**, 3728−3749.

(4) Gonçalves, R. A.; Baldan, M. R.; Ciapina, E. G.; Berengue, O. M. Nanostructured Pd/Sb2O3: A new and promising fuel cell electrocatalyst and non-enzymatic amperometric sensor for ethanol. *Appl. Surf. Sci.* **2019**, *491*, 9−15.

(5) Duan, H.; Wang, D.; Li, Y. Green chemistry for nanoparticle synthesis. *Chem. Soc. Rev.* **2015**, *44*, 5778−5792.

(6) Patzke, G. R.; Zhou, Y.; Kontic, R.; Conrad, F. Oxide nanomaterials: synthetic developments, mechanistic studies, and technological innovations. *Angew. Chem., Int. Ed.* **2011**, *50*, 826−859.

(7) Mao, Y.; Park, T.-J.; Zhang, F.; Zhou, H.; Wong, S. S. Environmentally friendly methodologies of nanostructure synthesis. *Small* **2007**, *3*, 1122−1139.

(8) Gupta, S. K.; Mao, Y. A review on molten salt synthesis of metal oxide nanomaterials: Status, opportunity, and challenge. *Prog. Mater. Sci.* **2021**, *117*, 100734.

(9) Khan, I.; Saeed, K.; Khan, I. Nanoparticles: Properties, applications and toxicities. *Arab. J. Chem.* **2019**, *12*, 908−931.

(10) Chen, X. Y.; Huh, H. S.; Lee, S. W. Hydrothermal synthesis of antimony oxychloride and oxide nanocrystals: Sb4O5Cl2, Sb8O11Cl2, and Sb2O3. *J. Solid State Chem.* **2008**, *181*, 2127−2132.

(11) Lakshmi, K.; Janas, K.; Shaijumon, M. Antimony oxychloride/graphene aerogel composite as anode material for sodium and lithium ion batteries. *Carbon* **2018**, *131*, 86−93.

(12) Shi, Y.; Wang, L.; Zhou, D.; Wu, T.; Xiao, Z. A Flower-Like Sb4O5Cl2 Cluster-based material as anode for potassium ion batteries. *Appl. Surf. Sci.* **2022**, *583*, 152509.

(13) Shi, Y.; Zhou, D.; Wu, T.; Xiao, Z. Deciphering the Sb4O5Cl2-MXene hybrid as a potential anode material for advanced potassium-ion batteries. *ACS Appl. Mater. Interfaces* **2022**, *14*, 29905−29915.

(14) Hu, X.; Chen, F.; Wang, S.; Ru, Q.; Chu, B.; Wei, C.; Shi, Y.; Ye, Z.; Chu, Y.; Hou, X.; Sun, L. Electrochemical performance of Sb4O5Cl2 as a new anode material in aqueous chloride-ion battery. *ACS Appl. Mater. Interfaces* **2019**, *11*, 9144−9148.

(15) Yang, L.; Huang, J.; Cao, L.; Shi, L.; Yu, Q.; Kong, X.; Jie, Y. pH-regulated template-free assembly of Sb4O5Cl2 hollow microsphere crystallites with self-narrowed bandgap and optimized photocatalytic performance. *Sci. Rep.* **2016**, *6*, No. 27765.

(16) Zhou, J.; Zhao, H.; Li, L.; Guo, L. Shape evolution of antimony oxychloride from sheaf-like to quasi-wafer structures. *Chin. Sci. Bull.* **2011**, *56*, 3817−3822.

(17) Peng, C.; Guo, J.; Yang, W.; Shi, C.; Liu, M.; Zheng, Y.; Xu, J.; Chen, P.; Huang, T.; Yang, Y. Synthesis of three-dimensional flower-like hierarchical ZnO nanostructure and its enhanced acetone gas sensing properties. *J. Alloys Compd.* **2016**, *654*, 371−378.

(18) Wang, L.; Wang, L.; Li, G.; Zhu, Y.; Liu, C.; Zeng, L.; Zhong, S.; Wang, L. J. Three-dimensional CuPc films decorated with well-ordered PVA parallel nanofiber arrays for low concentration detecting NO2 sensor. *Sens. Actuators, B* **2021**, *337*, 129781.

(19) Liu, M.; An, M.; Xu, J.; Liu, T.; Wang, L.; Liu, Y.; Zhang, J. Three-dimensional carbon foam supported NiO nanosheets as non-enzymatic electrochemical H2O2 sensors. *Appl. Surf. Sci.* **2021**, *542*, 148699.

(20) Li, B.; Li, Y.; Ma, P. Synthesis of different inorganic acids doped polyaniline materials and behavior of enhancing NH3 gas sensing properties. *Org. Electron.* **2023**, *114*, No. 106749, DOI: 10.1016/j.orgel.2023.106749.

(21) Sharma, A.; Rawal, I.; Rajpal, A.; Khokhar, A.; Kumar, V.; Goyal, P. K. Highly sensitive and selective room temperature ammonia sensor based on polyaniline thin film: in situ dip-coating polymerization. *J. Mater. Sci.: Mater. Electron.* **2022**, *33*, 14071−14085.

(22) Hsieh, C.-H.; Xu, L.-H.; Wang, J.-M.; Wu, T.-M. Fabrication of polypyrrole/tin oxide/graphene nanoribbon ternary nanocomposite and its high-performance ammonia gas sensing at room temperature. *Mater. Sci. Eng. B* **2021**, *272*, 115317.

(23) Wang, X. X.; Li, Z.; Yang, Y.; Tang, T.; Cheng, Y. F.; Xu, K.; Xie, H. G.; Chen, Y. L.; Cheng, L.; Tao, X. W.; et al. 3D substoichiometric MoO3- x/EGaln framework for room temperature NH3 gas sensing. *J. Alloys Compd.* **2023**, *939*, 168690.

(24) Tang, T.; Li, Z.; Cheng, Y. F.; Xu, K.; Xie, H. G.; Wang, X. X.; Hu, X. Y.; Yu, H.; Zhang, B. Y.; Tao, X. W.; et al. Single-step growth of p-type 1D Se/2D GeSe x O y heterostructures for optoelectronic NO 2 gas sensing at room temperature. *J. Mater. Chem. A* **2023**, *11*, 6361−6374.

(25) Zhuang, J.; Pan, H.; Feng, W. 3D urchin-like CoVO/MXene nanosheet composites for enhanced detection signal of nitrite. *Sens. Actuators, B* **2023**, *378*, 133207.

(26) Tang, T.; Li, Z.; Cheng, Y. F.; Xie, H. G.; Wang, X. X.; Chen, Y. L.; Cheng, L.; Liang, Y.; Hu, X. Y.; Hung, C. M.; et al. In-situ mechanochemically tailorable 2D gallium oxyselenide for enhanced optoelectronic NO2 gas sensing at room temperature. *J. Hazard. Mater.* **2023**, *451*, 131184.

(27) Gonçalves, R. A.; Toledo, R. P.; Joshi, N.; Berengue, O. M. Green synthesis and applications of ZnO and TiO2 nanostructures. *Molecules* **2021**, *26*, 2236.

(28) Kim, J.-W.; Porte, Y.; Ko, K. Y.; Kim, H.; Myoung, J.-M. Micropatternable double-faced ZnO nanoflowers for flexible gas sensor. *ACS Appl. Mater. Interfaces* **2017**, *9*, 32876−32886.

(29) Bigiani, L.; Zappa, D.; Maccato, C.; Gasparotto, A.; Sada, C.; Comini, E.; Barreca, D. Mn3O4 nanomaterials functionalized with Fe2O3 and ZnO: Fabrication, characterization, and Ammonia sensing properties. *Adv. Mater. Interfaces* **2019**, *6*, 1901239.

(30) Najim, A. A.; Darwoysh, H. H.; Dawood, Y. Z.; Hazaa, S. Q.; Salih, A. T. Structural, topography, and optical properties of Ba-doped Mn3O4 thin films for ammonia gas sensing application. *Phys. Status Solidi A* **2018**, *215*, 1800379.

(31) Xu, S.; Wang, J.; Lin, H.; Li, R.; Cheng, Y.; Sang, S.; Zhuo, K. ZnO/NiO nanofibers prepared by electrostatic spinning for rapid ammonia detection at room temperature. *Electron. Mater. Lett.* **2022**, *18*, 568−577.

(32) Wu, H.; Gong, X.; Tao, W.; Zhao, L.; Wang, T.; Liu, F.; Yan, X.; Sun, P.; Lu, G. Humidity-activated ammonia sensor based on

mesoporous AlOOH towards breath diagnosis. *Sens. Actuators, B* **2023**, *380*, No. 133322, DOI: 10.1016/j.snb.2023.133322.
(33) Wang, Y.; Liu, J.; Cui, X.; Gao, Y.; Ma, J.; Sun, Y.; Sun, P.; Liu, F.; Liang, X.; Zhang, T.; Lu, G. NH3 gas sensing performance enhanced by Pt-loaded on mesoporous WO3. *Sens. Actuators, B* **2017**, *238*, 473−481.
(34) Shao, S.; Xie, C.; Zhang, L.; Wei, S.; Kim, H. W.; Kim, S. S. CsPbI3 NC-Sensitized SnO2/Multiple-Walled Carbon Nanotube Self-Assembled Nanomaterials with Highly Selective and Sensitive NH3 Sensing Performance at Room Temperature. *ACS Appl. Mater. Interfaces* **2021**, *13*, 14447−14457.
(35) Zhao, Z.; Yang, H.; Wei, Z.; Xue, Y.; Sun, Y.; Zhang, W.; Li, P.; Gong, W.; Zhuiykov, S.; Hu, J. NH3 sensor based on 3D hierarchical flower-shaped n-ZnO/p-NiO heterostructures yields outstanding sensing capabilities at ppb level. *Sensors* **2020**, *20*, 4754.
(36) Santiago, S. R. M. S.; Wang, H.-J.; Chen, Y.-T.; Hsu, I.-J.; Wu, C.-B.; Hsu, K.-M.; Cheng, M.-C.; Lin, T.-N.; Feria, D. N.; Chou, W.-C.; Shen, J. L. Density-Dependent Carrier Recombination in MoS2 Quantum Dots and Its Implications for Luminescence Sensing of Ammonium Hydroxide. *ACS Appl. Nano Mater.* **2020**, *3*, 11630−11637.
(37) Gil, R. L.; Amorim, C. G.; Cuartero, M. Addressing the Detection of Ammonium Ion in Environmental Water Samples via Tandem Potentiometry-Ion Chromatography. *ACS Meas. Sci. Au* **2022**, *2*, 199−207.
(38) Acevedo-Correa, D.; Rodríguez-Meza, J. E.; Martelo, R. J. Effect of ammonium hydroxide on quality of meat products. *Contemp. Eng. Sci.* **2018**, *11*, 1513−1532.
(39) Pandeeswari, R.; Jeyaprakash, B. High sensing response of β-Ga2O3 thin film towards ammonia vapours: Influencing factors at room temperature. *Sens. Actuators, B* **2014**, *195*, 206−214.
(40) Harish, V.; Ansari, M. M.; Tewari, D.; Gaur, M.; Yadav, A. B.; García-Betancourt, M.-L.; Abdel-Haleem, F. M.; Bechelany, M.; Barhoum, A. Nanoparticle and Nanostructure Synthesis and Controlled Growth Methods. *Nanomaterials* **2022**, *12*, 3226.
(41) Lakshmi, K.; Janas, K.; Shaijumon, M. Antimony oxychloride embedded graphene nanocomposite as efficient cathode material for chloride ion batteries. *J. Power Sources* **2019**, *433*, 126685.
(42) Jiang, Q.; Yuan, X.; Wang, H.; Chen, X.; Gu, S.; Liu, Y.; Wu, Z.; Zeng, G. A facile hydrothermal method to synthesize Sb 2 S 3/Sb 4 O 5 Cl 2 composites with three-dimensional spherical structures. *RSC Adv.* **2015**, *5*, 53019−53024.
(43) Särnstrand, C. The crystal structure of antimony (III) chloride oxide Sb4O5Cl2. *Acta Crystallogr., Sect. B* **1978**, *34*, 2402−2407.
(44) Karakucuk, A.; Celebi, N. Investigation of formulation and process parameters of wet media milling to develop etodolac nanosuspensions. *Pharm. Res.* **2020**, *37*, 111.
(45) Qi, Y.; Zhang, J. Chemically modified Sb2O3, a new member of high solar-reflective material family, incorporating with ASA (acrylonitrile-styrene-acrylate copolymer) for fabrication of cooling composite with lower wetting behavior. *Composites, Part B* **2019**, *162*, 112−121.
(46) Jiang, Y.; Liu, J. Definitions of pseudocapacitive materials: a brief review. *Energy Environ. Mater.* **2019**, *2*, 30−37.
(47) Gogotsi, Y.; Penner, R. M. Energy storage in nanomaterials-capacitive, pseudocapacitive, or battery-like? *ACS Nano* **2018**, *12*, 2081−2083, DOI: 10.1021/acsnano.8b01914.
(48) Gileadi, E. Electrode kinetics for chemists, chemical engineers, and materials scientists. *Electrochim. Acta* **1993**, *40*, 2689 DOI: 10.1016/0013-4686(95)90077-2.
(49) Han, G.-Q.; Liu, Y.-R.; Hu, W.-H.; Dong, B.; Li, X.; Shang, X.; Chai, Y.-M.; Liu, Y.-Q.; Liu, C.-G. Crystallographic structure and morphology transformation of MnO2 nanorods as efficient electrocatalysts for oxygen evolution reaction. *J. Electrochem. Soc.* **2016**, *163*, H67.
(50) Li, X.; Fang, Y.; Lin, X.; Tian, M.; An, X.; Fu, Y.; Li, R.; Jin, J.; Ma, J. MOF derived Co 3 O 4 nanoparticles embedded in N-doped mesoporous carbon layer/MWCNT hybrids: extraordinary bi-functional electrocatalysts for OER and ORR. *J. Mater. Chem. A* **2015**, *3*, 17392−17402.
(51) Xia, L.; Song, H.; Li, X.; Zhang, X.; Gao, B.; Zheng, Y.; Huo, K.; Chu, P. K. Hierarchical 0D- 2D Co/Mo selenides as superior bifunctional electrocatalysts for overall water splitting. *Front. Chem.* **2020**, *8*, 382.
(52) Fukuhara, M.; Kuroda, T.; Hasegawa, F.; Shirai, Y.; Suwa, T.; Hashida, T.; Nishijima, M. Amorphous titanium-oxide supercapacitors with high capacitance. *Europhys. Lett.* **2019**, *128*, 58001.
(53) Wang, X.; Lu, Y.; Zhao, H.; Sun, Y.; Wang, R. Conductive electrodes of metallic-organic compound CH 3 CuS nanowires for all-solid-state flexible supercapacitors. *Nanoscale* **2021**, *13*, 6921−6926.
(54) Thomaz, D. V.; de Aguiar Filho, A. M.; De Macedo, I. Y. L.; Rodrigues, E. S. B.; Gil, E. D. S. Predictive modelling to study the electrochemical behaviour of PdO, TiO2 and perovskite-type LaFeO3 modified carbon paste electrodes. *Path Sci.* **2019**, *5*, 4001−4007.
(55) Solís, J. C.; Galicia, M. High Performance of MWCNTs-Chitosan Modified Glassy Carbon Electrode for Voltammetric Trace Analysis of Cd (II). *Int. J. Electrochem. Sci.* **2020**, *15*, 6815−6828, DOI: 10.20964/2020.07.56.
(56) Manna, S.; Kumar, S.; Sharma, A.; Sahoo, S.; Dey, M.; Mishra, P.; Satpati, A. rGO/ReO3 nano composite modified electrode for the ultra-sensitive determination of dopamine and uric acid. *Biosens. Bioelectron.: X* **2022**, *11*, 100156.
(57) da Silva, O. B.; Machado, S. A. Evaluation of the detection and quantification limits in electroanalysis using two popular methods: application in the case study of paraquat determination. *Anal. Methods* **2012**, *4*, 2348−2354.
(58) Rahman, M. M.; Jamal, A.; Khan, S. B.; Faisal, M. Characterization and applications of as-grown β-Fe 2 O 3 nanoparticles prepared by hydrothermal method. *J. Nanopart. Res.* **2011**, *13*, 3789−3799.
(59) Rahman, M. M.; Jamal, A.; Khan, S. B.; Faisal, M. CuO codoped ZnO based nanostructured materials for sensitive chemical sensor applications. *ACS Appl. Mater. Interfaces* **2011**, *3*, 1346−1351.
(60) Sazhin, S. G.; Soborover, E.; Tokarev, S. Sensor methods of ammonia inspection. *Russ. J. Nondestruct. Test.* **2003**, *39*, 791−806.
(61) Ji, X.; Banks, C. E.; Compton, R. G. The electrochemical oxidation of ammonia at boron-doped diamond electrodes exhibits analytically useful signals in aqueous solutions. *Analyst* **2005**, *130*, 1345−1347.
(62) Khan, S. B.; Rahman, M. M.; Jang, E. S.; Akhtar, K.; Han, H. Special susceptive aqueous ammonia chemi-sensor: Extended applications of novel UV-curable polyurethane-clay nanohybrid. *Talanta* **2011**, *84*, 1005−1010.
(63) Abaker, M.; Umar, A.; Baskoutas, S.; Dar, G.; Zaidi, S.; Al-Sayari, S.; Al-Hajry, A.; Kim, S.; Hwang, S. A highly sensitive ammonia chemical sensor based on α-Fe2O3 nanoellipsoids. *J. Phys. D: Appl. Phys.* **2011**, *44*, 425401.
(64) Baciu, A.; Manea, F.; Pop, A.; Pode, R.; Schoonman, J. Simultaneous voltammetric detection of ammonium and nitrite from groundwater at silver-electrodecorated carbon nanotube electrode. *Process Saf. Environ. Prot.* **2017**, *108*, 18−25.
(65) Merajin, M. T.; Nasiri, M.; Abedini, E.; Sharifnia, S. Enhanced gas-phase photocatalytic oxidation of n-pentane using high visible-light-driven Fe-doped WO3 nanostructures. *J. Environ. Chem. Eng.* **2018**, *6*, 6741−6748.
(66) Nadarajan, R.; Bakar, W. A. W. A.; Ali, R.; Ismail, R. Photocatalytic degradation of 1, 2-dichlorobenzene using immobilized TiO2/SnO2/WO3 photocatalyst under visible light: Application of response surface methodology. *Arab. J. Chem.* **2018**, *11*, 34−47.

https://doi.org/10.1021/acsomega.3c04751
ACS Omega 2023, 8, 41295−41301